

# In Silico-Driven THIOMAB Approach for Stable PROTAC Conjugates by Docking Payloads in Antibody Cavities

Shiwei Song, Yahui Liu, Jiaqi Liu, and Wanyi Tai\*



Cite This: <https://doi.org/10.1021/acs.bioconjchem.4c00588>



Read Online

ACCESS |



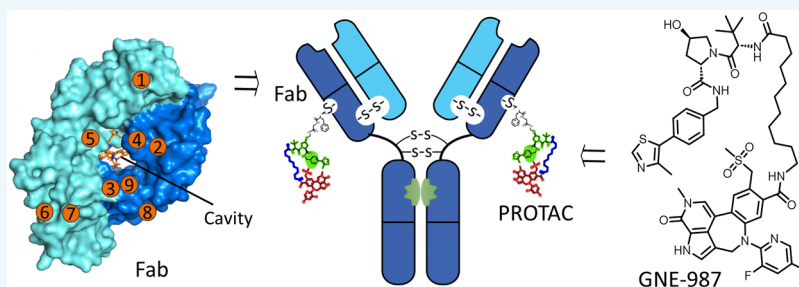
Metrics & More



Article Recommendations



Supporting Information



**ABSTRACT:** The heterobifunctional proteolysis targeting chimeras (PROTACs) are a class of emerging therapeutic modalities that enable selective degradation of target proteins in cells. As antibody payloads, they offer several advantages compared to conventional chemical toxins, such as catalytic nature, potent and long-lasting activity, and precise selectivity to avoid systemic toxicity. However, the relatively large size and high hydrophobicity of these chimeric payloads may result in challenging the stability of antibodies, which complicates the in vivo performance. In this work, we use the highly hydrophobic GNE-987 as model PROTAC to evaluate a THIOMAB approach for mitigating the conjugate's hydrophobicity while maintaining the therapeutic potency. We describe an *in silico* method to select the less hydrophobic site in an antibody and employ the stable tetrapeptide-aminomethoxy linker to conjugate the PROTAC payloads. The resulting degrader-antibody conjugate (J591 DAC) displays antigen-dependent BRD4 degradation and potent cytotoxic activity in PSMA-positive cancer cells. Finally, this DAC, bearing two highly hydrophobic PROTACs, also exhibits a long blood retention and strong antitumor efficacy in mouse models, likely owing to the homogeneous and stable conjugation from the THIOMAB approach. This work provides an example of the design and construction of antibody conjugates with highly hydrophobic payloads.

## INTRODUCTION

Therapeutic antibodies are now one of the most successful modalities to treat patients with cancers of various types. As the naturally occurring immunoglobulin, antibodies take advantage of the aberrant expression of antigens by tumor cells and distinguish them from normal tissues.<sup>1</sup> With the activation of host immune defense systems, antibody-labeled tumor cells could be eliminated by the effector functions such as complement-dependent cytotoxicity (CDC), antibody-dependent cellular cytotoxicity (ADCC), and regulation of T cell function.<sup>2,3</sup> Not only recognized as therapeutics itself, antibodies have also been envisioned as a drug carrier to pursue “magic bullets” that would specifically deliver therapeutic cargoes to recipient cells.<sup>4</sup> Various cargoes, such as toxic chemicals, RNA oligos, radionuclides, bioactive peptides, and CRISPR ribonucleoproteins, have been conjugated with antibodies and delivered to tumors.<sup>5–8</sup> Some toxin- and radionuclide-conjugated antibodies have been approved by the U.S. Food and Drug Administration (FDA), and many other conjugate types are evaluated in clinical trials.<sup>9,10</sup> It is predicted that the market size of antibody-drug conjugates (ADC) will rocket up to \$39 billion by 2030 due to

the growing demand for targeted therapy and increasing approval of new antibody conjugates by regulators.<sup>11</sup>

Among all of the payloads above, proteolysis targeting chimera (PROTAC) molecules are of particular interest to the pharmaceutical industry and academia for antibody conjugation, a modality known as a degrader-antibody conjugate (DAC). PROTACs are a type of heterobifunctional small molecules consisting of two distinct ligand components: one that specifically binds to the protein of interest (POI) and another that recruits an E3 ubiquitin ligase.<sup>12</sup> PROTACs can induce the formation of a ternary complex with POI and E3 ligase, which triggers the polyubiquitination and subsequent proteasome-mediated degradation of POI.<sup>13,14</sup> Compared to the chemical toxins such as auristatin, calicheamicin,

**Received:** December 24, 2024

**Revised:** March 24, 2025

**Accepted:** March 27, 2025

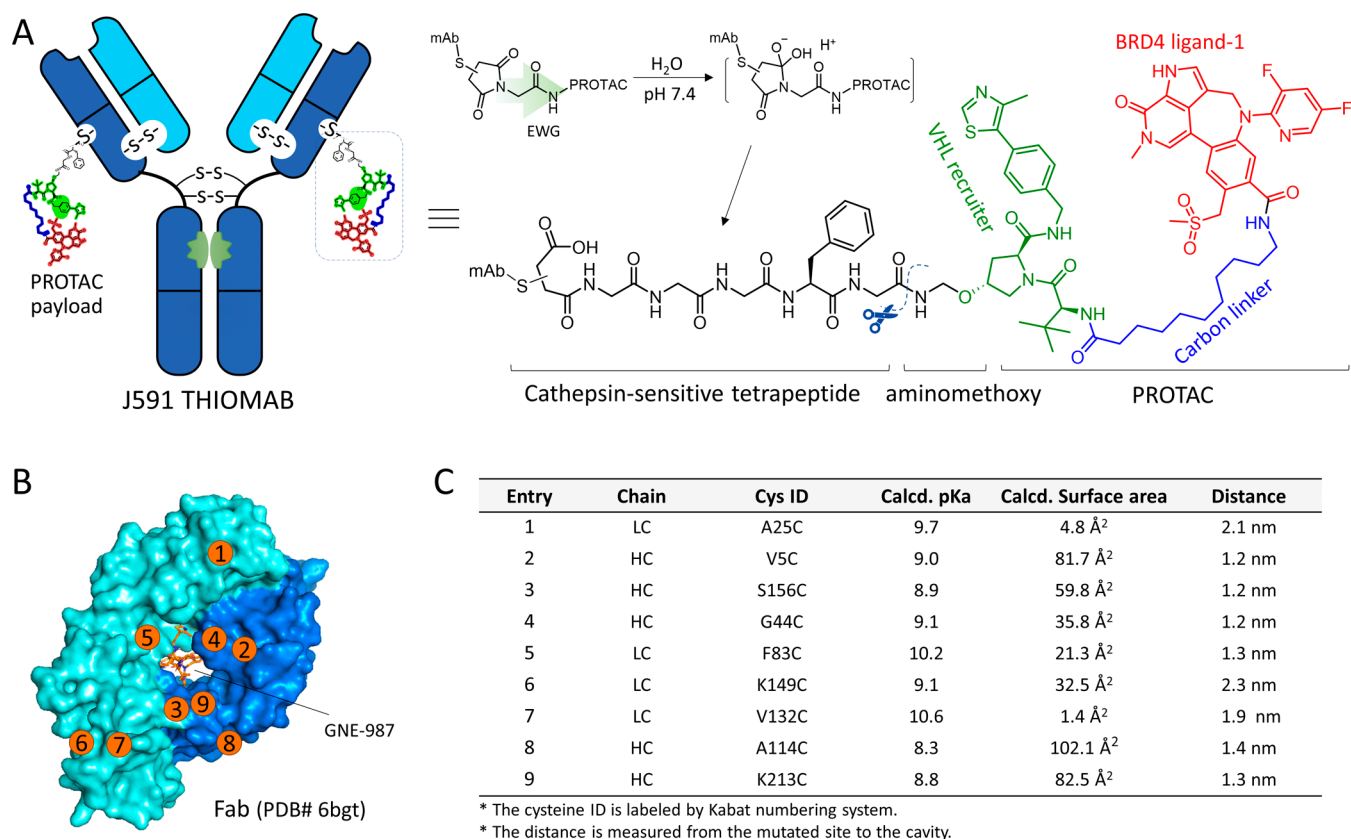


**Figure 1.** General scheme showing the conjugation of J591 THIOMAB with PROTAC GNE-987 via cathepsin-cleavable tetrapeptide-aminomethoxy linker. (A) PROTAC payloads are conjugated with the mutant cysteine HC-A114C of J591 to obtain a homogeneous DAR2 DAC. The maleimide–thiol linkage is in the ring-open form owing to the electron-withdrawing inductive effect from the carboxamido group (EWG). The scissor-cutting site indicates the cathepsin-cleavable position. (B) Docking of GNE-987 onto the Fab cavity. The potential sites of mutation are labeled by the cyclized numbers. (C) Table summarizing the *in silico* data of the cysteine sites.

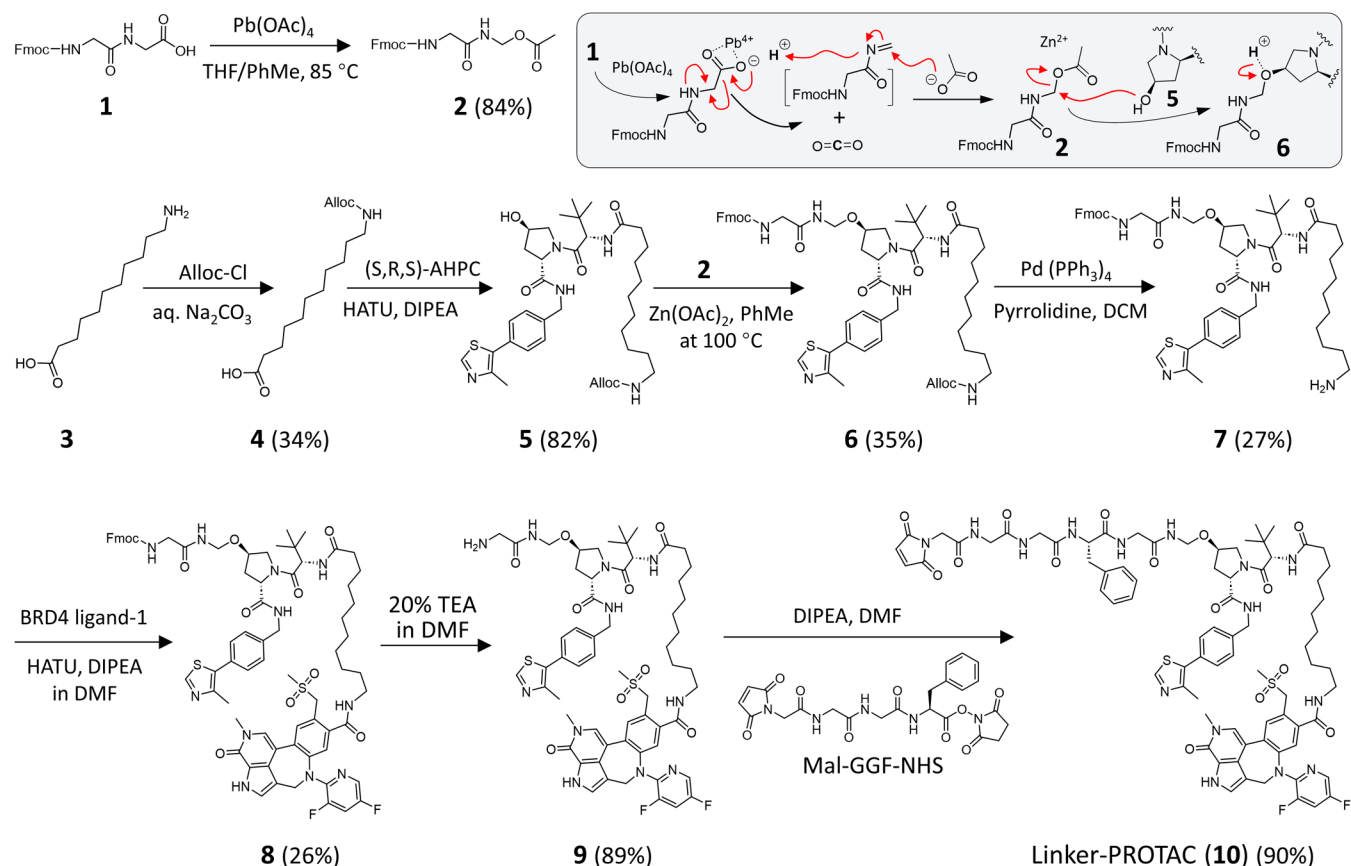
maytansine, and others commonly used in ADCs, PROTACs offer 3 major advantages which are particularly important for the concept of antibody conjugates: (i) the catalytic process enabling stoichiometric degradation of proteins: This nature bestows a single PROTAC molecule to degrade many copies of targeted proteins, which dramatically reduces the delivery burden of antibodies; (ii) degradation of the targeted protein instead of inhibition: Elimination of the disease-related proteins can prolong the pharmacological effect, which better fits the long dosing interval and pharmacokinetics of antibodies; and (iii) the precise targeting to the disease-related targets rather than cell-survival proteins (for example microtubule targeting by toxins) can minimize the toxicity to normal tissues, which increases the therapeutic index and clinical trial success rate.<sup>15</sup> Owing to these advantages, the development of DAC, even though still in its infancy, has attracted wide attention.<sup>16</sup> One main challenge facing DAC development is the relatively big size and high hydrophobicity of PROTAC payloads, which may cause the instability of antibodies and accelerate the clearance *in vivo*. In this regard, precise control of the payload number per antibody (drug-to-antibody ratio, DAR) at a low average is a prerequisite for the therapeutic efficacy of DAC.

In this study, we evaluated a THIOMAB antibody approach to develop the DAC for a very hydrophobic PROTAC GNE-987 (Figure 1). THIOMAB is a breakthrough technology that uses site-directed mutagenesis to incorporate cysteine (Cys) in

the antibody for a defined payload conjugation.<sup>17</sup> Monocysteine-engineered THIOMAB is the most popular platform and can yield dual-drug conjugation with near-uniform stoichiometry (DAR ~ 2), which might be the best for DAC development. GNE-987 is selected as DAC payloads in the study due to the extraordinary picomolar activity ( $DC_{50} \sim 0.02$  nM) and near-complete target degradation ( $D_{max} > 95\%$ ) in prostate cancer cell lines (unpublished data). GNE-987 is so far the most potent bromodomain-containing protein 4 (BRD4) degrader, but its physicochemical data (Mw 1096, clogD 5.6, aqueous solubility  $< 1 \mu\text{M}$ ) indicates that it is a highly hydrophobic PROTAC and might be challenging as antibody payloads.<sup>18</sup> Here, we used the *in silico* method to select a mutated Cysteine site in the THIOMAB scaffold of anti-PSMA (prostate-specific membrane antigen) antibody J591.<sup>19</sup> By using the GGFG tetrapeptide-aminomethoxy linker, we successfully conjugated GNE-987 to the heavy chains of J591 THIOMAB and obtained a homogeneous DAC with a DAR value close to 2. The THIOMAB-based DAC is highly specific and active in degrading the targeted proteins in prostate cancer cells. *In vivo* evaluation shows that the THIOMAB DAC can elicit a profound therapeutic effect in the mouse xenograft models despite the limited penetration in tumors.

## RESULTS AND DISCUSSION

***In Silico* Selection of Conjugate Sites on Antibody.** GNE-987 is a relatively large PROTAC payload, which would

Scheme 1. Synthesis of Linker-PROTAC 10<sup>a</sup>

<sup>a</sup>The isolated yields are given in parentheses after product IDs. The formation mechanism of the key aminomethoxy linkage is proposed in the gray box. The electron pushing arrows are shown in red.

introduce a hydrophobic patch to the context of the antibody and render the resulting DAC less stable. We proposed the monocysteine-engineered THIOMAB to control the drug load of two for the premise to reduce the hydrophobic burden and prevent the high DAR species that are prone to aggregate (Figure 1A). Besides the DAR control, our interest is also focused on the “site selection”, which describes a rational choice of possible conjugation sites to allow payloads to docking in the hydrophobic pocket of the antibody. It was previously reported that hydrophobic payloads such as pyrrolbenzodiazepine (PBD), monomethyl auristatin E (MMAE), and duocarmycin could be partially shielded by the antibody when the stable conjugation sites were selected.<sup>20–22</sup> In one elegant example, Coumans et al. have demonstrated that the hydrophobic linker-payload can position in the main cavity of Fab by hydrophobic interaction, yielding a less hydrophobic conjugate.<sup>23</sup> Encouraged by this discovery, we applied the *in silico* method to select a conjugate site for GNE-987 in the area of ~2 nm (linker length) distant from the cavity. Based on the crystal structure of the Fab template (PDB code 6bgt), 9 amino acid positions in the Fab were selected to substitute with cysteines (Figure 1B). The protein models of THIOMAB were generated using the mutagenesis wizard of PyMOL v3.1 (Figure S1), and the reactivity of each cysteine site was evaluated by calculating two important descriptors: cysteine residue (–SH) pK<sub>a</sub> and surface exposure area, which represent the residue’s nucleophilicity and accessibility to the maleimide-based linker-payload, respectively (Figure 1C).<sup>24</sup>

The PROPKA algorithm, a tool based on empirical calculation, revealed that cysteine HC-A114C (Kabat numbering) has the lowest pK<sub>a</sub> value (8.3), indicative of an ionizable thiolate state for Michael addition.<sup>25,26</sup> This reactive cysteine is also surface exposed, as predicted with a large accessible surface area of 102.1 Å<sup>2</sup> by the ASA v1.2 program. Accordingly, the HC-A114C mutant was constructed and expressed as the THIOMAB antibody for GNE-987 conjugation.

**Linker Design and Synthesis.** In order to conjugate with the corresponding THIOMAB, GNE-987 is activated with a thiol-reactive maleimide adduct and spaced by the GGFG tetrapeptide-aminomethoxy linkage (Figure 1). This linker is cathepsin-cleavable and has been used in the highly successful ADC drug DS8201a.<sup>27</sup> Compared to another popular linker ValCit-PABC, the GGFG tetrapeptidyl-aminomethoxy linker is less hydrophobic and more stable in mouse serum.<sup>28</sup> The reducing hydrophobicity helps producing a homogeneous ADC of high DAR (~8) in DS8201a.<sup>29</sup> The tetrapeptide here is chosen to mitigate the PROTAC hydrophobicity and separate it from the antibody. We believe that a spacer is helpful to alleviate the structure congestion and to ensure rapid PROTAC release in an active form by cathepsins in endosomes, as well.

The synthesis of linker-PROTAC 10 is depicted in Scheme 1. The synthetic route and selection of protecting groups center around the incorporation of an aminomethoxy linker in compound 6. This self-immolative linker is essential for free-PROTAC release, but its acid-labile feature makes the

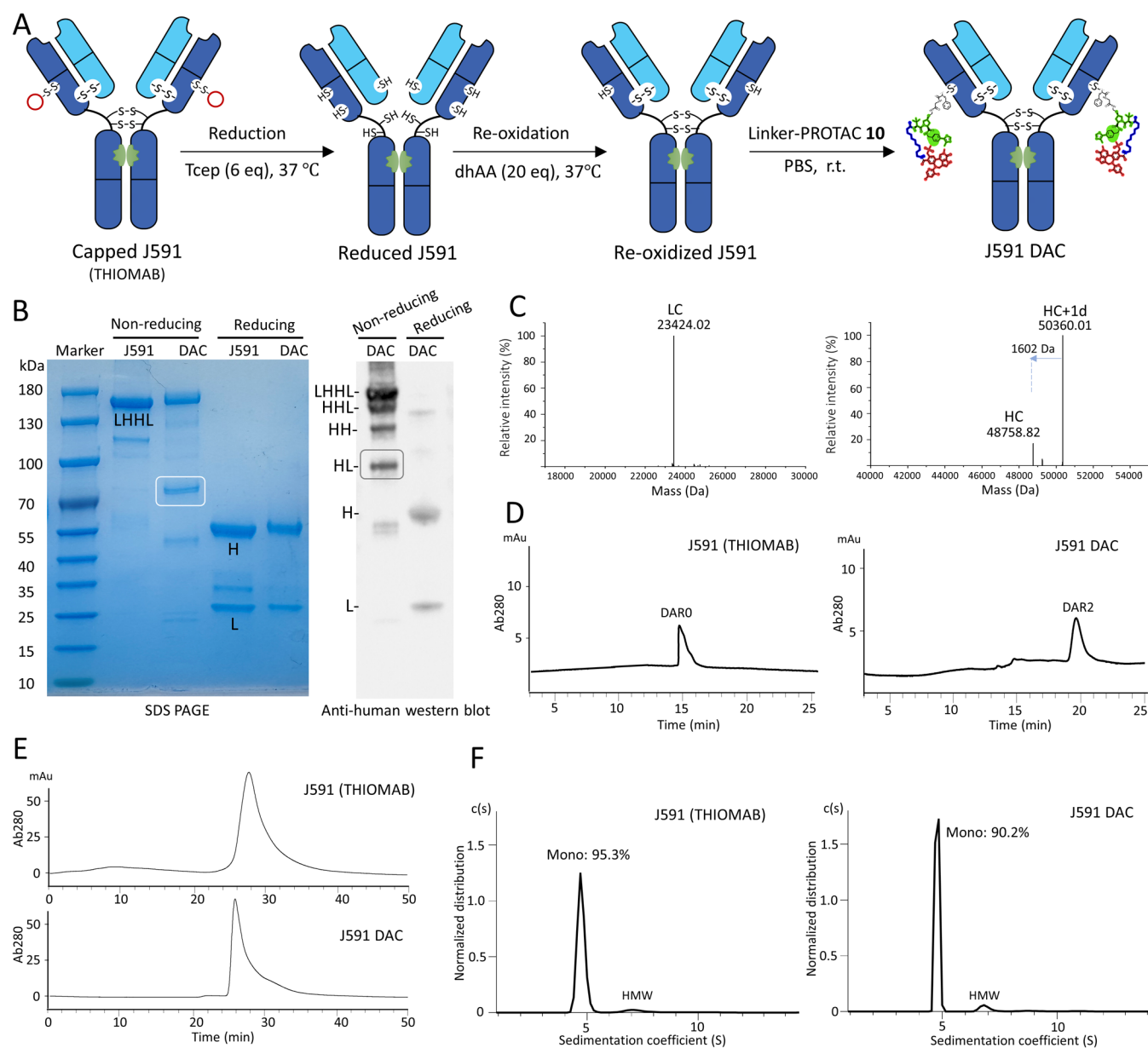


**Figure 2.** Synthesis and characterization of J591 DAC. (A) Conjugation of PROTAC payloads to the engineered THIOMAB cysteines using the reduction/oxidation protocol. The red cycles represent the capping adducts. (B) Characterization of THIOMAB J591 and DAC by SDS-PAGE. The intactness of antibodies is shown in a Western blotting image on the right. The bands of scrambled antibodies are marked by the rectangle. (C) Deconvoluted mass spectra of the light chain (LC) and PROTAC-appended heavy chain (HC+1d) from the DTT-reduced IdeS-digested J591 DAC. (D) HIC chromatograms showing the DAR species. (E) SEC analysis to characterize antibody aggregation. (F) Distribution profiles of antibody monomers (Mono) and aggregate species (HMW) generated by the AUC assay.

synthesis troublesome. The aminomethoxy linkage is introduced to the hydroxyl group of (S,R,S)-AHPC by an acid-catalyzed O-substitution of acetoxymethylamide **2**. This key intermediate **2** is readily synthesized by oxidative decarboxylation of compound **1** with  $\text{Pb}(\text{OAc})_4$  (lead tetraacetate), following a mechanism shown in the gray box of Scheme 1.<sup>30</sup> According to previous reports,<sup>31–34</sup> the acetoxy group behaves as a good leaving group and can be substituted by various nucleophiles including alcohols to obtain the aminomethoxy linkage. The nucleophilic substitution for the acetoxy group is generally facilitated by mild acids like pyridinium p-toluenesulfonate (PPTS).<sup>35</sup> However, the hydroxyproline in this case is a less nucleophilic alcohol, and stronger acids such as  $\text{Zn}(\text{OAc})_2$  (zinc acetate) or TFA (trifluoroacetic acid) are

applied to finish the title conversion. We use  $\text{Zn}(\text{OAc})_2$  in this route because it is mild and selective, which is more compatible with the acid-labile product. Compound **6** is then step-wisely coupled with BRD4 ligand-1 and tetrapeptide, producing the linker-PROTAC **10** in 4 steps and moderate yield. Reversed-phase high-performance liquid chromatography (RP-HPLC) analysis of **10** reveals that it has a retention time much longer than other antibody payloads, suggestive of its high hydrophobicity (Figure S2).

**Conjugation of PROTAC to THIOMAB with High Homogeneity.** Figure 2A illustrates the conjugation scheme of compound **10** to J591 THIOMAB. To activate the specific cysteine sites for PROTAC conjugation, THIOMAB J591 undergoes a reduction/oxidation procedure as reported

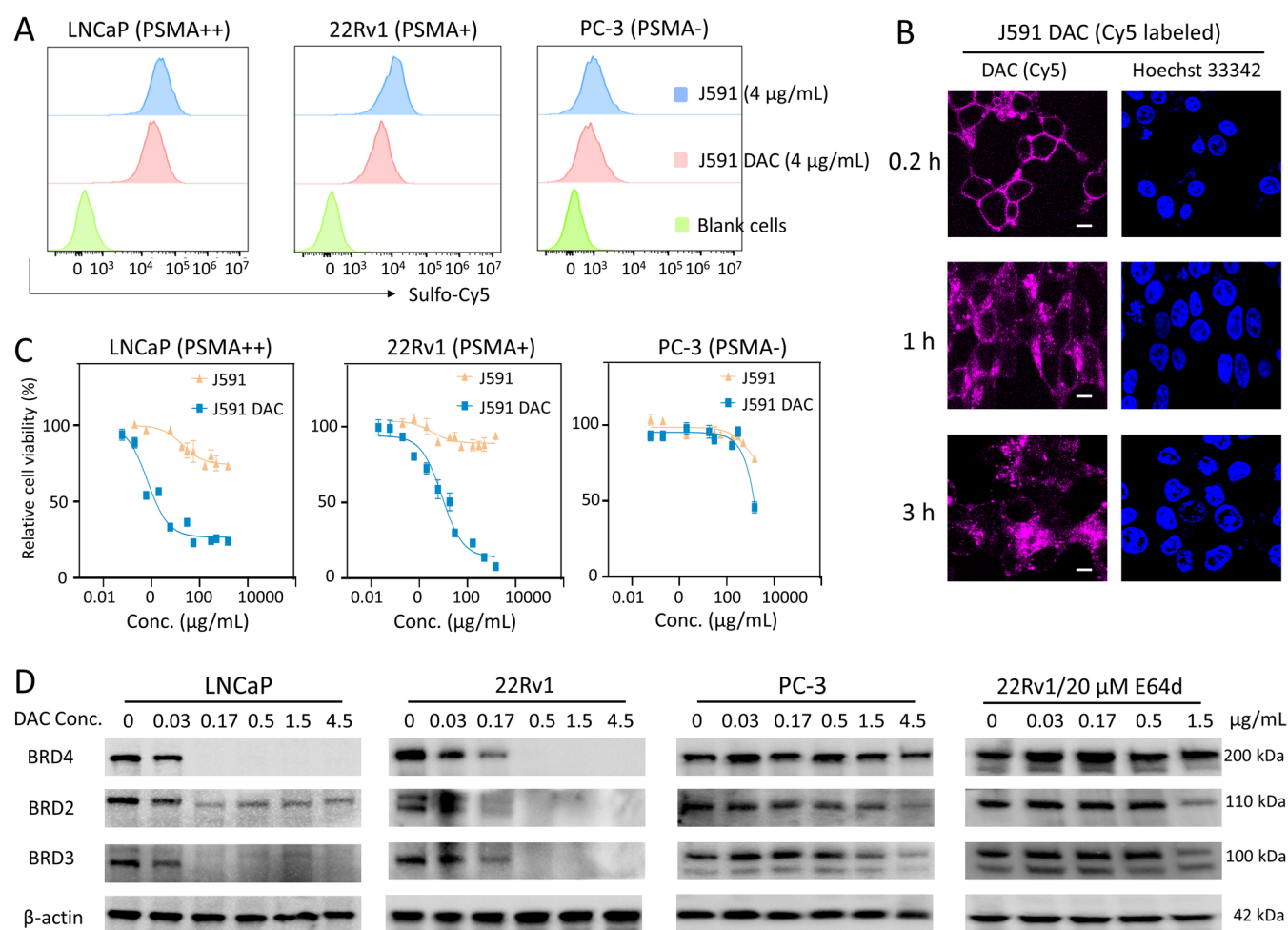


**Figure 3.** In vitro profiling of the bioactivities of anti-PSMA J591 DAC in LNCaP, 22Rv1, and PC-3 cells. (A) Flow plots showing the binding avidity to cancer cells in regard to PSMA expression levels. (B) Confocal imaging over time reveals the rapid internalization of sulfo-Cy5 labeled DAC in live 22Rv1 cells. Scale bar: 10  $\mu$ m. (C) Cell viability graphs profiled in three prostate cancer cell lines after treatment by J591 and DAC. (D) Western blotting images demonstrating the targeted degradation of BET proteins (BRD4, BRD2, and BRD3) by DAC. The proteolysis activity in 22Rv1 cells can be blocked by pan-cathepsin inhibitor E64d, which suppresses the tetrapeptide linker cleavage and PROTAC release.

previously.<sup>17</sup> Briefly, THIOMAB is fully reduced by tris(2-carboxyethyl) phosphine (TCEP) to remove the caps of engineered cysteines and reduce the interchain disulfide bonds at the same time. Subsequently, the native interchain disulfide bonds were rebridged by selective reoxidation with dehydroascorbic acid (dhAA). After this treatment, the unmasked cysteine was then coupled with compound **10** by thiol-maleimide chemistry but finally yielded a ring-open conjugation due to the inductive effect from the electron-withdrawing carboxamido group.<sup>36</sup> The efficient conjugation was demonstrated by SDS-PAGE and Western blotting (Figure 2B). Almost quantitative conjugation was observed by monitoring the band migration rate of heavy chains, whereas in nonreduced gels, we detected the presence of some scrambled antibody conjugates. This disulfide-scrambled product is formed by the incorrect reformation of disulfide bonds at the hinge region, resulting in the intrachain disulfide bridge rather than interchain bonds between two heavy chains.<sup>23</sup> It is believed that the side product is caused during the reoxidation by dhAA. More specific agents such as 2-(diphenylphosphino)benzenesulfonic acid (diPPBS) have been proposed to address this challenge.<sup>23</sup> LC/MS analysis shows that the linker-PROTAC is only distributed to the heavy chain (one drug per chain, HC+1d), confirming the predominant

conjugation at the engineered cysteine sites (Figure 2C). The result is in line with the data from analytical hydrophobic interaction chromatography (HIC), which determined an average DAR value close to 2 (Figure 2D). In order to evaluate the impact of payloads on antibody stability, we analyzed the percent abundance of high molecular weight (HMW) species (aggregate) using size exclusion chromatography (SEC) and analytical ultracentrifugation (AUC), respectively. As depicted in Figure 2E, the use of SEC gives the broad, diffuse, and anomalous peaks likely owing to the secondary interactions. In contrast, the AUC data well display the distribution percentages of antibody species versus sedimentation coefficient, in which the DAC shows only a lightly higher degree of aggregation than its parent THIOMAB antibody (Figure 2F). The favorable aggregation behavior of the THIOMAB approach is also demonstrated by comparing it with the DAC random (PROTACs are randomly conjugated to the reduced disulfide bonds of J591), as shown in Figure S3. Altogether, the results demonstrate that the THIOMAB approach produces a DAC conjugate with a homogeneous and stable structure.

**Selective Cell Killing and Target Proteolysis on Prostate Tumor Cells.** Given the extreme homogeneity of the THIOMAB DAC, we are very interested in evaluating its

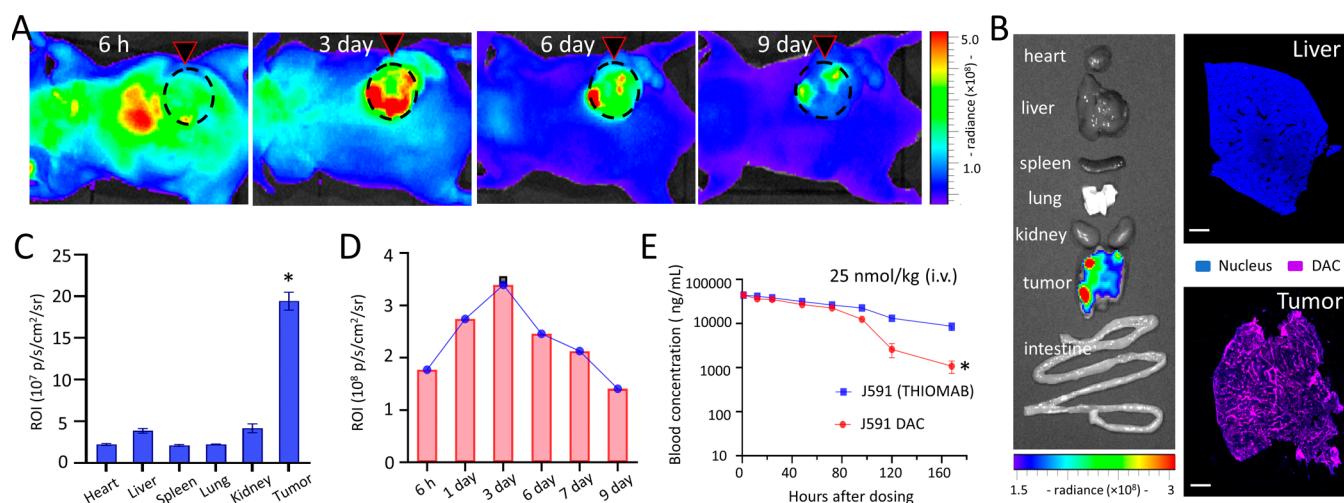


**Figure 4.** In vivo biodistribution and blood retention of J591 DAC in the 22Rv1 xenograft mouse models. (A) In vivo NIR fluorescence imaging of 22Rv1-tumor-bearing mice over 9 days. Red arrows indicate the tumor sites. (B) Ex vivo images of tissues and cryo-sections 9 days after tail-vein administration of DAC (sulfo-Cy5 labeled). Scale bar, 1 mm. (C) Quantitative analysis of fluorescence intensity remaining in ex vivo tissues. \*  $P < 0.05$ . (D) Dynamic intensity of DAC fluorescence in tumors. (E) Pharmacokinetics of J591 DAC and the parent THIOMAB in mice. \*  $P < 0.05$ .

bioactivities in tumor cells. Three human prostate cancer cell lines were selected on the basis of their PSMA expression status: LNCaP with a high level of PSMA expression (PSMA+), 22Rv1 showing moderate expression (PSMA+), and PSMA-negative PC-3 cells (PSMA-). Comparative plots of the avidity of three cell lines in Figure 3A show that J591 DAC displays a comparable antigen-binding capability to the parent J591 THIOMAB, indicating the neglectable impact of PROTAC conjugation on antibody affinity. We then moved the binding experiment to a 37 °C incubator and monitored the intracellular trafficking of DAC after receptor recognition (Figure 3B). A series of confocal images clearly show that Cy5 labeled DAC is initially associated with membrane receptors but internalized into cells quickly in a couple of hours, which is encouraging because rapid internalization is important to payload release and DAC activity. The  $IC_{50}$  values of J591 DAC are below 10  $\mu\text{g/mL}$  in the PSMA-positive LNCaP and 22Rv1 cells (Figure 3C). Compared to the naked THIOMAB antibody, the potency to tumor cells is augmented over a hundred times by PROTAC payloads in DAC. Moreover, we also observed a cell selectivity of toxicity depending on PSMA expression levels; for example, J591 DAC is more effective in LNCaP cells ( $IC_{50}$  0.7  $\mu\text{g/mL}$ ), whereas PC-3 is less affected ( $IC_{50} > 500 \mu\text{g/mL}$ ).

We subsequently conducted Western blotting experiments to determine whether the activity observed above was due to BRD4 degradation. As shown in Figure 3D, J591 DAC exhibits the robust degradation of BRD4 proteins in the PSMA-positive LNCaP and 22Rv1 cells. More than 95% BRD4 in 22Rv1 cells can be degraded at a DAC concentration as low as 0.5  $\mu\text{g/mL}$ . The degradation activity in LNCaP cells is even more profound, which is in agreement with the PSMA expression level. It is interesting to find that other bromodomain and extraterminal (BET) proteins, for example, BRD2 and BRD3, have also been targeted by J591 DAC. The degradation activity to pan-BET proteins likely stems from the payload GNE-987 because most BRD4 PROTACs simultaneously degrade all three BRD proteins, thereby increasing drug toxicity.<sup>37</sup> The treatment by J591 DAC is accompanied by a downregulation of c-Myc protein (Figure S4), a cancer-related gene down-

stream of the BET pathway and associated with cancer cell proliferation.<sup>38</sup>

It is worth noting that the linker cleavage (GGFG) by cathepsins is essential to the PROTAC release from DAC and the subsequent proteolysis (seen in Figure 3D). In order to prove its important role, we tried to block its cleavage with a pan-cathepsin inhibitor, E64d, and evaluated the impact on BET proteolysis by Western blotting. E64d is a membrane-permeable cysteine protease inhibitor that blocks the cathepsins' activity in acidic endo/lysosomal compartments and reduces the PROTAC payload release in its active form, thereby attenuating the DAC potency. When E64d is coincubated with 22RV1 cells, J591 DAC loses its capacity to degrade BET proteins, reflective of the cathepsin sensitivity of GGFG linkers. It is worth noting that the payload GNE-987 itself is more potent than J591 DAC and the DAC random when plotting  $IC_{50}$  in molar concentrations (Figure S5), which indicates that the payload release by cathepsin is a rate-limiting step, and efforts to improve linker sensitivity may boost DAC potency in the future.

**In Vivo Antitumor Activity of the PROTAC-Conjugated THIOMAB.** Lyon et al. reported that the hydrophobic payloads tend to be recognized by Kupffer cells in the liver and increase the clearance of ADC conjugates.<sup>39,40</sup> In our case, we minimized the drug loads per antibody by the THIOMAB approach, but this effort might be counteracted by the high hydrophobicity of GNE-987. In order to evaluate the impact on clearance, we labeled the J591 DAC with sulfo-Cy5 fluorescent probe and tracked its distribution, clearance, and tumor retention in mice. As shown in Figure 4A, DAC is located mainly in the liver at 6 h after administration. However, the accumulation of drugs in tumors continues to increase until the third day, after which the tumor fluorescence decays over time but remains detectable even at day 9 (Figure 4B,C). Quantitative analysis of the signal intensity in tumors over time confirms the trend (Figure 4D). In order to obtain more insight into the phenomenon, a pharmacokinetic study was carried out to obtain information about the time frame of DAC exposure to tumors in mice. As shown in Figure 4E, the DAC shows a shorter half-life ( $T_{1/2}$ ) than the parent THIOMAB antibody, indicative of the negative impact of payloads on

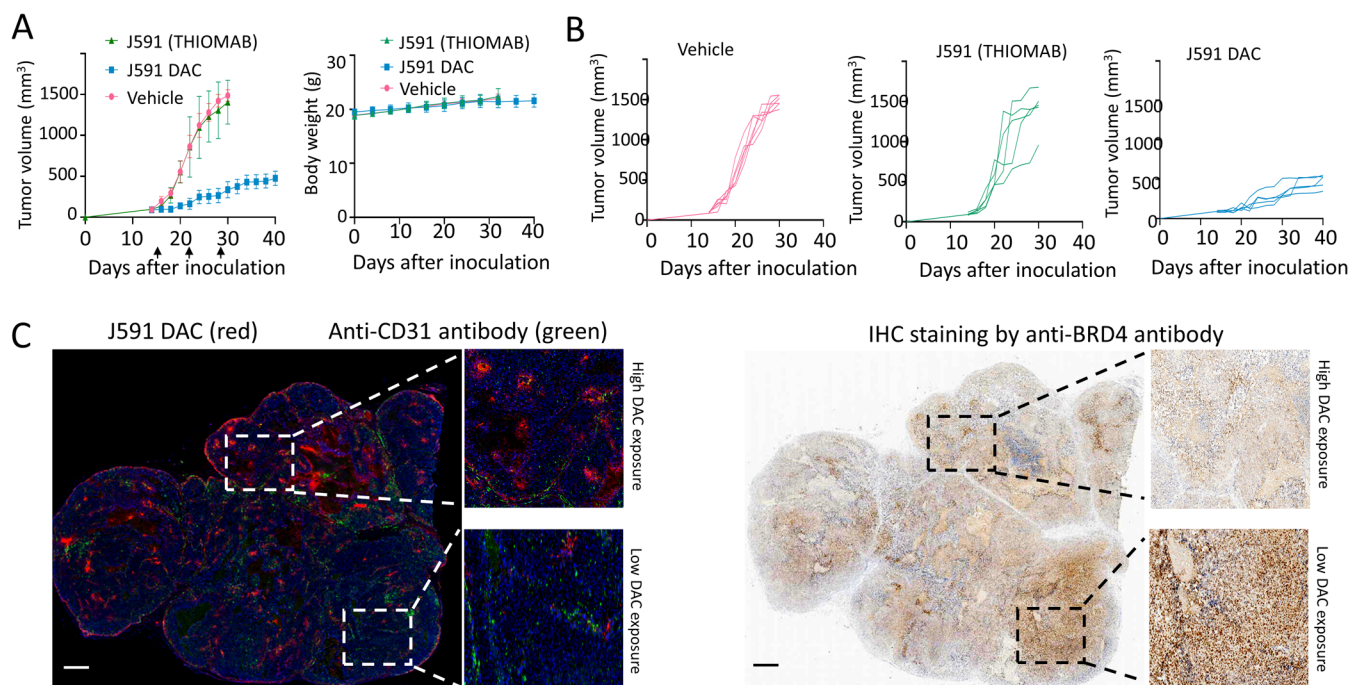


**Figure 5.** Evaluation of therapeutic efficacy and penetration in mouse xenograft models. (A) Graphs showing the tumor-growth (left) and body-weight (right) profiles after treatment by antibodies. The arrows indicate the day of injections. (B) Growth curves of individual tumors treated by vehicle control (left), J591 THIOMAB (middle), and its PROTAC conjugate (right). (C) Correlation between DAC penetration and targeted protein (BRD4) degradation in tumor sections at 3 days after tail-vein injection. J591 DAC and anti-CD31 antibody were labeled by sulfo-Cy5 and AF488, respectively. Scale bar, 1 mm.

clearance. The  $T_{1/2}$  value of DAC is around 80 h, which is in line with the time frame of DAC accumulation in tumors and the corresponding high blood exposure.

We then set up a prostate xenograft model to evaluate the *in vivo* efficacy of J591 DAC in mice and compared it to the parent anti-PSMA J591 antibody. The treatment regimen involves the administration of DAC at a dosage of 6 mg/kg via intravenous (*i.v.*) route when the tumor burden reaches approximately 100 mm<sup>3</sup>. As depicted in Figure 5A,B, the administration of multiple doses of DAC results in a significant inhibition of tumor growth in the 22Rv1 xenograft model. The robust therapeutic response observed in the treated group suggests that THIOMAB-based DAC has a potent antitumor effect against PSMA-positive tumors, which correlates well with the observation of activity *in vitro*. We notice that the body weight of the mice remained stable throughout the experimental period, a sign of the absence of acute toxicity after treatment.

Tissue penetration is one of the major challenges facing antibody-based therapeutics for solid tumors. Other than the small organic drugs, antibodies bear a high molecular weight (~150 kDa) and produce only restricted tumor penetration in regions around tumor vasculature, known as the “binding site barrier” (BSB) phenomenon.<sup>41</sup> The bystander effect is beneficial for payloads themselves to reach deeper tissue, but the change of topochemistry by the hydrophobic payloads and the corresponding impact on antibody penetration are unknown. We labeled the J591 DAC with the sulfo-Cy5 probe and visualized the spatial distribution of DAC in tumor tissue using the CaseViewer slide scanner. As shown in Figure 5C, DAC is limited in the tumor periphery (edge) and perivascular region of the tumor interior, resulting in suboptimal and heterogeneous tumor exposure. The drug

distribution in tumor sections is well-located with the fingerprint of immunohistochemical (IHC) slides showing the BRD4 protein degradation. The J591 DAC in this study exhibits limited penetration similar to that of the perivascular distributed J591-AF680 antibody reported by Nessler et al.<sup>42</sup> The DAC does not show any increase in penetration at later times, consistent with the BSB hypothesis that antibodies extravasate from the blood vessel and saturate the surrounding cell layers of the tumor nest, thereby forming a stalled saturation front and preventing deeper penetration over time.<sup>43</sup> Several strategies such as coadministration of parent antibodies, increment of dose and frequency, and affinity tuning have been proposed to improve tumor penetration of antibody conjugates,<sup>44–47</sup> which might apply to this THIOMAB J591 DAC.

## CONCLUSIONS

Targeted protein degradation by small-molecule PROTACs is a breakthrough technology in drug discovery, enabling the selective elimination rather than inhibition of specific protein targets. One PROTAC candidate ARV-471 has completed phase 3 clinical trial and received the FDA fast-track designation for the treatment of ER+/HER2- metastatic breast cancer.<sup>48</sup> Despite being promising, PROTACs have no selectivity, which degrades the proteins of not only cancer cells but also normal tissue cells. Moreover, many PROTAC molecules have poor pharmaceutical properties and low bioavailability. As a popular drug carrier, antibodies might conjugate with PROTACs and overcome these limitations. This strategy, known as DAC, has been explored by several research groups using various linkers and conjugation modalities.<sup>49</sup> For example, researchers from Wuxi Aptec utilized carbonate and pyrophosphate diester linkers to conjugate

antibodies and hydroxyproline moiety of VHL ligands;<sup>50</sup> Dragovich et al. extensively engineered the PROTAC spacer and introduced an aminophenyl site for antibody conjugation;<sup>51</sup> Orum therapeutics and other sections replaced the PROTAC payload with smaller molecular glues to reduce the antibody burden and hydrophobicity.<sup>52</sup>

As an example, we used PROTAC GNE-987 as payloads and constructed an anti-PSMA DAC using the THIOMAB approach. This strategy enables DAC to achieve a defined conjugation (DAR  $\sim$  2) and stable physiochemistry, leading to exceptional targeting selectivity and efficient degradation of BET proteins in PSMA-positive cancer cells. In vivo, DAC retains long-circulating pharmacokinetic properties and displays strong deposition in tumor sites. Furthermore, this DAC exhibits strong antitumor activity in vivo and effective BRD4 proteolysis in tumor tissues. In summary, our results support the rational choice of conjugation sites and precise control of DAR at a low average in the DAC development. We demonstrate that THIOMAB is a feasible approach for developing stable and bioactive DACs, even using highly hydrophobic PROTAC molecules as payloads.

## EXPERIMENTAL METHODS

**Cell Lines.** 22RV1, LNCaP, and PC-3 cells were purchased from the American Type Culture Collection (ATCC). HEK 293F cell was obtained from Thermo Fisher Scientific (Waltham). Roswell Park Memorial Institute (RPMI) 1640 medium, fetal bovine serum (FBS), and other cell culture supplementary reagents were purchased from Procell Inc. (Wuhan, China). Upon thawing, all adherent cells were cultured in RPMI 1640 medium supplemented with 10% FBS and 1% penicillin-streptomycin. The suspension HEK 293F cells were cultured in chemically defined Union-293 expression media from Union Biotech (Shanghai, China). All cells were cultured at 37 °C with 5% CO<sub>2</sub> and regularly checked for the absence of mycoplasma.

**In Silico Selection of Conjugation Sites.** The crystal structure of the Fab fragment (PDB ID: 6bgt) is used as the model for prediction. The molecular docking study is performed using AutoDock tools (version 1.5.7) to predict the interaction between GNE-987 and the Fab cavity. Ten conformational poses of GNE-987 are generated during the docking simulation. The resulting poses are ranked based on their binding free energy. The most stable binding mode is identified by selecting the lowest-energy conformation, which has a calculated binding energy of  $-6.58$  kcal/mol. The single-point mutation is introduced in the mode in a range of  $<2$  nm distant from the docking site. Nine amino acid positions in the Fab are selected for cysteine substitution. The indicated residue is mutated to cysteine and generates a THIOMAB model using the mutagenesis wizard in the PyMOL molecular graphics system (version 3.1). To predict the reactivity of engineered cysteines, we calculated the  $pK_a$  and solvent-accessible area. The  $pK_a$  of the thiol group in cysteines was predicted using the PROPKA algorithm (version 2.0). PROPKA estimates  $pK_a$  based on approximate perturbative terms, including desolvation of the residue, inter-residue Coulombic interactions, and hydrogen bonding interactions, which are parametrized on the default setting. The surface accessibility, quantified as the solvent-accessible surface area ( $\text{\AA}^2$ ) through geometric calculations, is calculated in ASA software (version 1.2, Center for Informational Biology, Ochanomizu University). The algorithm for the calculation

sets the maximum area ( $\text{\AA}^2$ ) for all amino acid residues. For cysteine in the GCG sequence, the maximal area is  $143.79 \text{\AA}^2$ . All of the predicted data are summarized in Figure 1C. PyMOL is used to measure the distance from the mutated site to the docking cavity.

**Antibody Expression.** The heavy chain and light chain genes of J591 mutant HC-A114C (Eu numbering) were cloned into a P1316-IgG1 expression vector with dual CMV promoters. The THIOMAB plasmid was amplified in a TOP 10 *Escherichia coli* host and isolated using the QIAGEN maxiprep kit. The day before transfection, HEK 293F cells were seeded at a density of  $1.5 \times 10^6$  cells/mL in fresh Union-293 media (100 mL). To prepare the transfection polyplex,  $125 \mu\text{g}$  of plasmid (diluted in 5 mL of Opti-MEM) and  $400 \mu\text{g}$  of PEI MAX (diluted in 5 mL of Opti-MEM) were mixed and incubated at 37 °C for 5 min, and then, the mixture was added to the culture. The suspension cells were shaken at a speed of 110 rpm at 37 °C in 5% CO<sub>2</sub>. Twenty hours later, sodium butyrate was added at a final concentration of 10 mM, followed by supplementing glucose at a final concentration of 50 mM. Five days after transfection, the culture was harvested by centrifugation. The antibody in the supernatant was purified by protein A chromatography. The eluted antibody was exchanged to PBS by a Sephadex G-25 desalting column.

**Conjugation of Antibody and PROTAC.** For J591 DAC construction, Linker-PROTAC 10 (the synthetic method is available in Supporting Information) is conjugated to the cysteine residue at position A114C of THIOMAB J591 through maleimide chemistry. To activate the capped cysteine sites, THIOMAB J591 was reduced with 10 equiv TCEP at 37 °C for 1 h. The TCEP was removed by the Sephadex G-25 desalting column, followed by adding DHAA to a final concentration of 1 mM to rebridge the default disulfide bond. DHAA was removed by the Sephadex G-25 desalting column. The engineered cysteine was free to react with the linker-PROTAC 10 by incubating with 2.5 equiv linker-PROTAC 10 in PBS buffer at room temperature for 3 h. The maleimide–thiol linkage can be hydrolyzed into the ring-open form simultaneously during the payload conjugation. The free linker-PROTAC was removed by the Sephadex G-25 desalting column, and the purified J591 DAC was obtained. The extent of conjugation was characterized by reverse-phase LC-MS after deglycosylation.

**HIC Analysis.** To determine the DAR value, the J591 DAC and its control THIOMAB J591 were analyzed using a SHIMADZU LC-40D HPLC system equipped with a Tosoh TSKgel Butyl-NPR hydrophobic interaction chromatography (HIC) column ( $4.6 \times 100 \text{ mm}^2$ ,  $5 \mu\text{m}$ , TOSOH Bioscience). Elution condition was as follows: mobile phase A = 25 mM sodium phosphate including 1.5 M ammonium sulfate (pH 7.0); mobile phase B = 25 mM sodium phosphate containing 20% isopropanol (pH 7.0); gradient over 30 min from 0 to 100% B; 100% buffer B adjusted to 100% buffer A from 30 to 35 min, maintained 100% buffer A from 35 to 40 min; flow rate = 0.5 mL/min.

**SEC Analysis.** THIOMAB J591 and J591 DAC were assessed via the size exclusion chromatography (SEC) on TSKgel SuperSW mAb HR  $7.8 \text{ mm} \times 30 \text{ cm}$ ,  $4 \mu\text{m}$ . Prior to injection in SEC, all samples were centrifuged at 8000 g to eliminate insoluble species. The chromatography condition was as follows: mobile phase: 200 mM sodium phosphate (pH 6.7) plus 5% acetonitrile (to minimize the secondary interaction); flow rate: 0.3 mL/min; 20  $\mu\text{L}$  injections with

1.0 mg/mL THIOMAB J591 and J591 DAC, and the elution signal was detected at 280 nm using a Ultraviolet/visible (UV/vis) detector.

**Analytical Ultracentrifugation (AUC) Assay.** The THIOMAB J591 and J591 DAC were diluted to 0.5 mg/mL in PBS buffer prior to loading into AUC cells. For the sedimentation velocity AUC, samples (0.390 mL) were loaded into the sample channel of AUC cells having quartz windows and 12 mm double-sector Epon centerpieces. The sample buffer (PBS, 0.400 mL) was loaded into the corresponding reference channel of each cell. The centrifugation was carried out at 16 °C and 36000 rpm using the Beckman Optima AUC. Radial scans of the concentration profile were collected sequentially by absorbance at 280 nm until no further sedimentation was observed. The resulting data sets were analyzed by using the program SEDFIT with a continuous  $c(s)$  distribution model, yielding best-fit distributions for the number of sedimenting species.

**Confocal Imaging.** 22RV1 (10,000 cells) were seeded in confocal dishes. After overnight culture, the culture was changed with 1 mL of fresh culture media (10% FBS), followed by adding 10  $\mu\text{g}/\text{mL}$  of J591 DAC (the drug can be labeled by sulfo-Cy5 NHS). After incubation at 37 °C in 5%  $\text{CO}_2$  (0.2, 1, and 3 h), Hoechst 33342 (Millipore sigma, B2261) was added to stain the cell nucleus for 1 h at 37 °C. The cell membrane was then counter-stained with WGA-AF594 (Invitrogen, W11262) for 2 min. The monolayer was washed twice with DPBS and imaged with confocal laser scanning microscopy (Leica).

**Cell Viability Assay.** 22RV1, LNCaP, and PC-3 cells ( $3 \times 10^3$  /well) were seeded in 96-well plates at a density of  $3 \times 10^3$  per well. After overnight culture, cells were treated with DAC conjugates or an antibody control for 72 h. The viable cells in the 96-well plate were counted using the CCK8 assay (Beyotime, #C0038). The  $\text{IC}_{50}$  was profiled using GraphPad Prism 9.4.1.

**Cell Binding and Flow Cytometry Analysis.** To assess the binding specificity to PSMA, all experiments were performed at room temperature to minimize internalization upon receptor recognition. Briefly, J591 DAC or THIOMAB J591 (sulfo-Cy5 labeled, Duofluor) was diluted within the same concentration (4  $\mu\text{g}/\text{mL}$ ) and coincubated with cancer cells (100,000 cells) for 2 h in RPMI 1640 media supplemented with 10% FBS. The cells were washed twice with PBS and analyzed on a BD LSR II flow cytometer (Beckton Dickinson).

**Western Blotting Analysis.** The cells were inoculated in 6-well plates at a density of  $3 \times 10^5$  cells per well and incubated for 12 h. Following this, cells were treated with either DMSO or specified concentrations of antibodies for a designated period. After the incubation, the culture medium was discarded. The tumor cells were washed with PBS and lysed with IP buffer (Beyotime P0013). The lysate was centrifuged at 13,000 rpm for 10 min at 4 °C. The supernatant was collected, and protein concentration was determined using a BCA Assay Kit (Thermo A55860). Protein samples (5–20  $\mu\text{g}$ ) were loaded onto a 8% sodium dodecyl sulfate-polyacrylamide gel (ACE Biotechnology ET12420Gel) and subjected to electrophoresis at 120 V for 1.5 h. Proteins were then transferred to an immobilized PVDF membrane (Millipore IPVH00010). The membrane was blocked with 5% BSA for 1–2 h and incubated with primary antibodies overnight at 4 °C or 1.5 h at room temperature. The

membrane was washed 3–4 times with TBST (Tris-buffered saline with Tween 20), each wash lasting 5 min. Following this, the membrane was incubated with HRP-conjugated secondary antibodies at room temperature for 1 h, washed 3 times with TBST (each wash lasting 8 min), and treated with ECL-enhanced HRP substrate (Proteintech PK10001). Chemiluminescence was detected using a ChemiDoc XRS+ gel imaging system (Bio-Rad). The primary antibodies used were anti-BRD4 (1:3000 dilution, CST#13440), anti-BRD3 (1:100 dilution, Santa Cruz sc-81202), anti-BRD2 (1:3000 dilution, NatureBios A95996), anti-c-Myc (1:3000 dilution, Abmart T55150), and anti- $\beta$ -actin (1:5000 dilution, 81115-1-RR). The secondary antibody HRP-conjugated Goat anti-Rabbit IgG, ABclonal, AS014, 1:10,000; HRP-conjugated Goat anti-Mouse IgG, ABclonal, AS003, 1:10,000. HRP-conjugated anti-Human IgG, Proteintech, SA00001-17, 1:5000. The markers used were SmartBuffer Prestained Protein ladder (N6619, 10–250 kDa).

**Mouse Xenograft Establishment.** Animal studies were conducted under the approval of the Experimental Animal Management Committee of Wuhan University. All of the animal studies were performed in compliance with the guidelines of the Chinese Regulations for the Administration of Affairs Concerning Experimental Animals and the Institutional Animal Care and Use Committee of Wuhan University. The model was established by the transplantation of 22Rv1 ( $5 \times 10^6$ ) cells in the 1:1 mixture of RPMI 1640 and Matrigel that were subcutaneously injected into the 6-week-old male BALB/c nude mice. When the average tumor volume reached approximately 100  $\text{mm}^3$ , the mice were selected on the basis of tumor volume and body weight and randomly assigned to experimental groups with five or six animals per group. Tumor volumes and body weights were measured 2–3 times per week, and tumor volumes were calculated as per the formula  $[\text{length}/2] \times [\text{width}^2]$ .

**In Vivo Biodistribution.** The biodistribution study was performed when the tumor volume reached 400  $\text{mm}^3$ . J591 DAC (sulfo-Cy5 labeled, 25 nmol/kg) were injected into mice via the tail vein in a volume of 150  $\mu\text{L}$ . Mice were then imaged using the In-Vivo Xtreme II imaging system (Bruker) at selected time points (6 h, day 1, day 3, day 7, and day 9). At the end of the experiment, the mice were euthanized. The dissected tumors and major organs (heart, liver, spleen, lung, kidney, and intestine) were imaged.

**Pharmacokinetic Studies.** For pharmacokinetic studies, BALB/C mice were injected with either THIOMAB J591 (25 nmol/kg) or J591 DAC (25 nmol/kg, sulfo-Cy7 labeled, equal dye dose) bioconjugates. Approximately 30  $\mu\text{L}$  of blood was collected via the posterior orbital venous plexus at selected time points (1, 12, 24, 48, 72, 96, 120, and 168 h). The fluorescence remaining in blood samples was imaged and quantified using an Odyssey CLx imaging system (LI-COR Biosciences).

**Antitumor Therapy in Mice.** When the average tumor volume reached approximately 100  $\text{mm}^3$ , the mice were selected based on tumor volume and randomly assigned to groups of 5–6 animals per group. The compounds J591 DAC and THIOMAB J591 were dissolved in PBS and administrated at a dosage of 6 mg/kg (QW, 3 injections). PBS was used as the vehicle control. During the whole experimental period, both tumor dimensions and mouse body weight were meticulously measured. Tumor volumes and body weights

were measured 2–3 times per week, and tumor volumes were calculated as per the formula  $[\text{length}/2] \times [\text{width}^2]$ .

**Fluorescence Macroscopic Imaging of Tissue Sections.** The tumor-bearing BALB/c mice were injected i.v. with 25 nmol/kg J591 DAC (sulfo-Cy5 labeled). The mice were sacrificed at selected time points. The livers and tumors were removed, and a portion of the liver and whole tumor were fixed overnight at 4 °C with 10% formalin (Sigma-Aldrich). Fixed tissues were embedded in Tissue-Tek OCT Compound (Sakura), sliced into 20- $\mu\text{M}$  sections, and mounted on pretreated glass slides with Fluoroshield plus DAPI histology mounting medium (Sigma-Aldrich). Sections were evaluated for the presence of conjugates by using the 3DHISTECH CaseViewer Panoramic Scanner.

**Immunohistochemical Analysis of BRD4 Degradation in Tumor Sections.** To verify the BRD4 protein degradation in vivo, the tumor-bearing mice were treated with J591 DAC (sulfo-Cy5 labeled) at a single dose of 6 mg/kg. At selected time points after tail-vein injection, the tumors were harvested, sectioned into frozen slices, and stained with anti-BRD4 antibody (1:1000 dilution, CST#13440) for IHC analysis.

**Tissue Penetration Evaluation.** Tumor-bearing BALB/c-nu mice were injected intravenously with 6 mg/kg J591 DAC (sulfo-Cy5 labeled). Tumors were dissected, fixed, frozen in OCT, and stored at  $-80$  °C until cryostat sectioning into 15  $\mu\text{m}$  slices. Blood vessels were stained using antimouse CD31 antibody labeled with AlexaFluor488 for 30 min. The slides were then mounted with a Fluoroshield plus DAPI histology mounting medium (Sigma-Aldrich). The slides were then imaged using a 3DHISTECH CaseViewer panoramic scanner with a 200 $\times$  objective (laser source 488, 450, and 649 nm).

**Statistical Analysis.** The mean  $\pm$  standard deviation (SD) was used to report all data. GraphPad Prism software was used to conduct the statistical comparisons using the student's *t* test as  $*P < 0.05$ ,  $**P < 0.01$ . A difference of  $*P < 0.05$  was considered significant.

## ■ ASSOCIATED CONTENT

### SI Supporting Information

The Supporting Information is available free of charge at <https://pubs.acs.org/doi/10.1021/acs.bioconjchem.4c00588>.

3D structures of the Fab protein models used for *in silico* prediction; HPLC spectra of linker-payloads; aggregation analysis of the randomly conjugated DAC; western blotting; IC<sub>50</sub> profiles of cells treated by GNE-987 and J591 DAC random; antibody sequence information; synthetic methods and spectra for all compounds (PDF)

## ■ AUTHOR INFORMATION

### Corresponding Author

Wanyi Tai – Department of Pharmaceutical Engineering, School of Pharmaceutical Sciences, Wuhan University, Wuhan, Hubei 430071, China; [orcid.org/0000-0003-3589-8263](https://orcid.org/0000-0003-3589-8263); Email: [wanyi-tai@whu.edu.cn](mailto:wanyi-tai@whu.edu.cn)

### Authors

Shiwei Song – Department of Pharmaceutical Engineering, School of Pharmaceutical Sciences, Wuhan University, Wuhan, Hubei 430071, China

Yahui Liu – Department of Pharmaceutical Engineering, School of Pharmaceutical Sciences, Wuhan University, Wuhan, Hubei 430071, China

Jiaqi Liu – Department of Pharmaceutical Engineering, School of Pharmaceutical Sciences, Wuhan University, Wuhan, Hubei 430071, China

Complete contact information is available at:

<https://pubs.acs.org/10.1021/acs.bioconjchem.4c00588>

### Notes

The authors declare no competing financial interest.

## ■ ACKNOWLEDGMENTS

This work was financially supported by the National Key R&D Program of China (Grant No. 2021YFA0909900) and the National Natural Science Foundation of China (Grant No. 82273860).

## ■ REFERENCES

- (1) Di Meo, F.; Kale, B.; Koomen, J. M.; Perna, F. Mapping the cancer surface proteome in search of target antigens for immunotherapy. *Mol. Ther.* **2024**, *32* (9), 2892–2904.
- (2) Moquist, P. N.; Zhang, X.; Leiske, C. I.; Eng-Duncan, N. M. L.; et al. Reversible Chemical Modification of Antibody Effector Function Mitigates Unwanted Systemic Immune Activation. *Bioconjugate Chem.* **2024**, *35* (6), 855–866.
- (3) Wang, H.; Song, J.; Quan, Y.; Liu, J.; Tai, W.; et al. Chemically Programmed Fc Protein as Antibody Mimetic to Targeting Carbonic Anhydrase IX. *Bioconjugate Chem.* **2024**, *35* (10), 1459–1467.
- (4) Aigbogun, O. P.; Phenix, C. P.; Krol, E. S.; Price, E. W. The Chemistry of Creating Chemically Programmed Antibodies (cPabs): Site-Specific Bioconjugation of Small Molecules. *Mol. Pharmaceutics* **2023**, *20* (2), 853–874.
- (5) Elgundi, Z.; Reslan, M.; Cruz, E.; Sifniotis, V.; et al. The state-of-play and future of antibody therapeutics. *Adv. Drug Delivery Rev.* **2017**, *122*, 2–19.
- (6) You, J.; Zhang, J.; Wang, J.; Jin, M. Cysteine-Based Coupling: Challenges and Solutions. *Bioconjugate Chem.* **2021**, *32* (8), 1525–1534.
- (7) Petruzzella, A.; Bruand, M.; Santamaria-Martinez, A.; Katanayeva, N.; et al. Antibody–peptide conjugates deliver covalent inhibitors blocking oncogenic cathepsins. *Nat. Chem. Biol.* **2024**, *20* (9), 1188–1198.
- (8) Cochran, M.; Arias, D.; Burke, R.; Chu, D.; et al. Structure–Activity Relationship of Antibody–Oligonucleotide Conjugates: Evaluating Bioconjugation Strategies for Antibody–siRNA Conjugates for Drug Development. *J. Med. Chem.* **2024**, *67* (17), 14852–14867.
- (9) Dean, A. Q.; Luo, S.; Twomey, J. D.; Zhang, B. Targeting cancer with antibody–drug conjugates: Promises and challenges. *mAbs* **2021**, *13* (1), No. 1951427.
- (10) Flynn, P.; Suryaprakash, S.; Grossman, D.; Panier, V.; et al. The antibody–drug conjugate landscape. *Nat. Rev. Drug Discovery* **2024**, *23* (8), 577–578.
- (11) Bhushan, A.; Misra, P. Economics of Antibody Drug Conjugates (ADCs): Innovation, Investment and Market Dynamics. *Curr. Oncol. Rep.* **2024**, *26* (10), 1224–1235.
- (12) Churcher, I. Protac-Induced Protein Degradation in Drug Discovery: Breaking the Rules or Just Making New Ones? *J. Med. Chem.* **2018**, *61* (2), 444–452.
- (13) Sun, D.; Zhang, J.; Dong, G.; He, S.; et al. Blocking Non-enzymatic Functions by PROTAC-Mediated Targeted Protein Degradation. *J. Med. Chem.* **2022**, *65* (21), 14276–14288.
- (14) Chen, S.; Mao, Q.; Cheng, H.; Tai, W. RNA-Binding Small Molecules in Drug Discovery and Delivery: An Overview from Fundamentals. *J. Med. Chem.* **2024**, *67* (18), 16002–16017.
- (15) Mahalingaiah, P. K.; Ciurlionis, R.; Durbin, K. R.; Yeager, R. L.; et al. Potential mechanisms of target-independent uptake and toxicity of antibody–drug conjugates. *Pharmacol. Ther.* **2019**, *200*, 110–125.

- (16) New guise ADCs couple antibodies to degraders *Nat. Biotechnol.* **2023**, Vol. 41 10, p 1360.
- (17) Junutula, J. R.; Raab, H.; Clark, S.; Bhakta, S.; et al. Site-specific conjugation of a cytotoxic drug to an antibody improves the therapeutic index. *Nat. Biotechnol.* **2008**, 26 (8), 925–932.
- (18) Pillow, T. H.; Adhikari, P.; Blake, R. A.; Chen, J.; et al. Antibody Conjugation of a Chimeric BET Degradator Enables in vivo Activity. *ChemMedChem* **2020**, 15 (1), 17–25.
- (19) Smith-Jones, P. M.; Vallabahajosula, S.; Goldsmith, S. J.; Navarro, V.; et al. In vitro characterization of radiolabeled monoclonal antibodies specific for the extracellular domain of prostate-specific membrane antigen. *Cancer Res.* **2000**, 60 (18), 5237–5243.
- (20) Ohri, R.; Bhakta, S.; Fourie-O'Donohue, A.; dela Cruz-Chuh, J.; et al. High-Throughput Cysteine Scanning To Identify Stable Antibody Conjugation Sites for Maleimide- and Disulfide-Based Linkers. *Bioconjugate Chem.* **2018**, 29 (2), 473–485.
- (21) Tumey, L. N.; Li, F.; Rago, B.; Han, X.; et al. Site Selection: a Case Study in the Identification of Optimal Cysteine Engineered Antibody Drug Conjugates. *AAPS J.* **2017**, 19 (4), 1123–1135.
- (22) Sussman, D.; Westendorf, L.; Meyer, D. W.; Leiske, C. I.; et al. Engineered cysteine antibodies: an improved antibody-drug conjugate platform with a novel mechanism of drug-linker stability. *Protein Eng. Des. Sel.* **2018**, 31 (2), 47–54.
- (23) Coumans, R. G. E.; Ariaans, G. J. A.; Spijker, H. J.; Verkerk, P. R.; et al. A Platform for the Generation of Site-Specific Antibody–Drug Conjugates That Allows for Selective Reduction of Engineered Cysteines. *Bioconjugate Chem.* **2020**, 31 (9), 2136–2146.
- (24) Marino, S. M.; Gladyshev, V. N. Analysis and functional prediction of reactive cysteine residues. *J. Biol. Chem.* **2012**, 287 (7), 4419–4425.
- (25) Awoonor-Williams, E.; Rowley, C. N. Evaluation of Methods for the Calculation of the pKa of Cysteine Residues in Proteins. *J. Chem. Theory Comput.* **2016**, 12 (9), 4662–4673.
- (26) Awoonor-Williams, E.; Golosov, A. A.; Hornak, V. Benchmarking In Silico Tools for Cysteine pKa Prediction. *J. Chem. Inf. Model.* **2023**, 63 (7), 2170–2180.
- (27) Ogitani, Y.; Aida, T.; Hagihara, K.; Yamaguchi, J.; et al. DS-8201a, A Novel HER2-Targeting ADC with a Novel DNA Topoisomerase I Inhibitor, Demonstrates a Promising Antitumor Efficacy with Differentiation from T-DM1. *Clin. Cancer Res.* **2016**, 22 (20), 5097–5108.
- (28) Dorywalska, M.; Dushin, R.; Moine, L.; Farias, S. E.; et al. Molecular Basis of Valine-Citrulline-PABC Linker Instability in Site-Specific ADCs and Its Mitigation by Linker Design. *Mol. Cancer Ther.* **2016**, 15 (5), 958–970.
- (29) Xu, Z.; Guo, D.; Jiang, Z.; Tong, R.; et al. Novel HER2-Targeting Antibody-Drug Conjugates of Trastuzumab Beyond T-DM1 in Breast Cancer: Trastuzumab Deruxtecan (DS-8201a) and (Vic)-Trastuzumab Duocarmazine (SYD985). *Eur. J. Med. Chem.* **2019**, 183, No. 111682.
- (30) Nachbauer, L.; Brückner, R. Synthesis of a C–C+6 Building Block Common to Important Polyol, Polyene Antibiotics from a Divinylcarbinol by a Desymmetrizing Sharpless Epoxidation. *Eur. J. Org. Chem.* **2013**, 2013 (29), 6545–6562.
- (31) Hashimoto, M.; Niwata, S.; Iwata, S.; Fukami, H. A Facile Synthesis of Substituted Methylamides from Acetoxymethylamides. *Chem. Express* **1992**, 7, 65–68.
- (32) Le Diguarher, T.; Orturno, J.-C.; Shanks, D.; Guilbaud, N.; et al. Synthesis of N,N'-disubstituted 3-aminobenzo[c] and [d]azepin-2-ones as potent and specific farnesyl transferase inhibitors. *Bioorg. Med. Chem. Lett.* **2004**, 14 (3), 767–771.
- (33) Hashimoto, M.; Niwata, S.; Fukami, H.; Iwata, S.; et al. Synthesis and Herbicidal Activity of Pyridinyloxyphenoxypropionamides. *Biosci. Biotechnol. Biochem.* **1992**, 56 (9), 1448–1450.
- (34) Labanauskas, L.; Mazeikaite, R.; Striela, R.; Gedrimaite, O.; et al. Nucleophilic substitution of the acetoxy group in 3-methylbenzoylaminomethyl acetate. *Russ. Chem. Bull.* **2011**, 60 (8), 1672–1676.
- (35) Qin, G.; Zhang, T. Y.; Chen, G.; Song, P. H. et al. Exatecan Derivatives, Linker-Payloads, and Conjugates and Thereof. U.S. Patent US11814394B2, 2022.
- (36) Fontaine, S. D.; Reid, R.; Robinson, L.; Ashley, G. W.; Santi, D. V. Long-term stabilization of maleimide-thiol conjugates. *Bioconjugate Chem.* **2015**, 26 (1), 145–152.
- (37) Zengerle, M.; Chan, K.-H.; Ciulli, A. Selective Small Molecule Induced Degradation of the BET Bromodomain Protein BRD4. *ACS Chem. Biol.* **2015**, 10 (8), 1770–1777.
- (38) Raina, K.; Lu, J.; Qian, Y.; Altieri, M.; et al. PROTAC-induced BET protein degradation as a therapy for castration-resistant prostate cancer. *Proc. Natl. Acad. Sci. U.S.A.* **2016**, 113 (26), 7124–7129.
- (39) Lyon, R. P.; Bovee, T. D.; Doronina, S. O.; Burke, P. J.; et al. Reducing hydrophobicity of homogeneous antibody-drug conjugates improves pharmacokinetics and therapeutic index. *Nat. Biotechnol.* **2015**, 33 (7), 733–735.
- (40) Meyer, D. W.; Bou, L. B.; Shum, S.; Jonas, M.; et al. An in Vitro Assay Using Cultured Kupffer Cells Can Predict the Impact of Drug Conjugation on in Vivo Antibody Pharmacokinetics. *Mol. Pharmacol.* **2020**, 17 (3), 802–809.
- (41) van Dongen, G. A. Improving Tumor Penetration of Antibodies and Antibody-Drug Conjugates: Taking Away the Barriers for Trojan Horses. *Cancer Res.* **2021**, 81 (15), 3956–3957.
- (42) Nessler, I.; Khera, E.; Vance, S.; Kopp, A.; et al. Increased Tumor Penetration of Single-Domain Antibody-Drug Conjugates Improves In Vivo Efficacy in Prostate Cancer Models. *Cancer Res.* **2020**, 80 (6), 1268–1278.
- (43) Lu, G.; Nishio, N.; van den Berg, N. S.; Martin, B. A.; et al. Co-administered antibody improves penetration of antibody-dye conjugate into human cancers with implications for antibody-drug conjugates. *Nat. Commun.* **2020**, 11 (1), No. 5667.
- (44) Singh, A. P.; Guo, L.; Verma, A.; Wong, G. G.-L.; Thurber, G. M.; Shah, D. K. Antibody Coadministration as a Strategy to Overcome Binding-Site Barrier for ADCs: a Quantitative Investigation. *AAPS J.* **2020**, 22 (2), No. 28.
- (45) Rubahamya, B.; Dong, S.; Thurber, G. M. Clinical translation of antibody drug conjugate dosing in solid tumors from preclinical mouse data. *Sci. Adv.* **2024**, 10 (22), No. eadk1894.
- (46) Cilliers, C.; Menezes, B.; Nessler, I.; Linderman, J.; Thurber, G. M. Improved Tumor Penetration and Single-Cell Targeting of Antibody-Drug Conjugates Increases Anticancer Efficacy and Host Survival. *Cancer Res.* **2018**, 78 (3), 758–768.
- (47) Rudnick, S. I.; Lou, J.; Shaller, C. C.; Tang, Y.; et al. Influence of Affinity and Antigen Internalization on the Uptake and Penetration of Anti-HER2 Antibodies in Solid Tumors. *Cancer Res.* **2011**, 71 (6), 2250–2259.
- (48) Chirnomas, D.; Hornberger, K. R.; Crews, C. M. Protein degraders enter the clinic - a new approach to cancer therapy. *Nat. Rev. Clin. Oncol.* **2023**, 20 (4), 265–278.
- (49) Hong, K. B.; An, H. Degradator-Antibody Conjugates: Emerging New Modality. *J. Med. Chem.* **2023**, 66 (1), 140–148.
- (50) Dragovich, P. S.; Adhikari, P.; Blake, R. A.; Blaquiére, N.; et al. Antibody-mediated delivery of chimeric protein degraders which target estrogen receptor alpha (ER $\alpha$ ). *Bioorg. Med. Chem. Lett.* **2020**, 30 (4), No. 126907.
- (51) Dragovich, P. S.; Pillow, T. H.; Blake, R. A.; Sadowsky, J. D.; et al. Antibody-Mediated Delivery of Chimeric BRD4 Degradators. Part 2: Improvement of In Vitro Antiproliferation Activity and In Vivo Antitumor Efficacy. *J. Med. Chem.* **2021**, 64 (5), 2576–2607.
- (52) Poudel, Y. B.; Thakore, R. R.; Chekler, E. P. The New Frontier: Merging Molecular Glue Degradator and Antibody-Drug Conjugate Modalities To Overcome Strategic Challenges. *J. Med. Chem.* **2024**, 67 (18), 15996–16001.